Studies Related to Attenuation of PGA and Liquefaction Potential for Earthquakes ($M_s > 6.0$) in the New Madrid Seismic Zone

14-08-0001-G1999

Chandan K Saikia
Woodward-Clyde Consultants,
566 El Dorado Street,
Pasadena, CA 91101
(818) 449-7650.

Objective

The New Madrid seismic zone generated a series of great earthquakes in 1811-1812 and existing tectonic features indicate its capability for future large earthquakes (Nuttli, 1973; 1983). Several other earthquakes with m_b between 5.3 and 6.2 have followed the 1811-1812 events in recent time (Nuttli et al., 1979). Due to the lack of instrumental recording of strong motion data from large earthquakes in the central United States (CUS), the currently available attenuation relations for the peak ground accelerations (PGA) are derived by extrapolating small events to the large magnitude range using a point-source model (Nuttli, 1973) and random vibration theory (RVT) (Boore and Atkinson, 1987; Toro and McGuire, 1987). The purpose of this project is to develop improved attenuation relations for PGA, particularly in the large magnitude range ($M_w > 6.0$) in CUS using synthetic accelerograms obtained by a simulation technique that incorporates an accurate wave-propagation model and an extended fault model. The wave propagation method can account for the important crustal reflections such as the critical reflection from the Moho observed in the San Francisco Bay region during the 1989 Loma Prieta earthquake (Somerville and Yoshimura, 1990; McGarr et al., 1991). The response of these reflections is inaccurately represented by the geometrical wave propagation method used in the earlier studies.

Simulation of Ground Motion

To develop attenuation relations, we have simulated ground motions at 168 sites (Figure 1) which encompass the entire New Madrid fault zone using a semi-empirical method (Somerville et al., 1991) for earthquakes of magnitude $M_w = 6.5$, $M_w = 7.0$ and $M_w = 7.5$. The fault size and seismic moment of each earthquake were defined based on a chosen source scaling law. Following the representation theorem of elastodynamics, the fault surface is discretized into many sub-faults, each treated as a small earthquake. The contributions from these sub-faults are synthesized by convolving empirical source functions with a theoretical medium response. They are then lagged and summed. The present method uses the accelerograms from an aftershock of the 1979 Imperial Valley earthquake as empirical source functions to represent source radiation. The response of the recording site effect from these accelerograms was removed adopting the procedure discussed in Somerville et al. (1991). In addition, we did not apply a kappa correction to these source functions since the kappa estimates from the source functions are similar to the kappa values noted from the limited CUS strong-motion data (Herrmann, personal communication, 1989). The wave propagation is represented by the response of direct P, S and reflected phases (Figure 2) from interfaces with

strong impedance contrast of a crustal model of the New Madrid fault zone chosen from Saikia et al. (1990). This crustal model was developed by modeling weak motion earthquake data recorded in the distance range of 40 and 180 km from the Saint Louis University network. In Figure 2, we show the locations of three sources marked by "X" and various rays leaving the sources to a common receiver. The fault is buried at a depth of 0.6 km with a depth extension to 15 km. The fault was given a strike of 220°, a dip of 70°, and a rake of 110°.

It was pointed out by Boore and Atkinson (1987) and Toro and McGuire (1987) that ground motions predicted by the increasing stress-drop model of Nuttli (1973) were inconsistent with the available ground motion data. Their investigations suggested that a constant stress-drop law (Somerville et al. 1987) is likely to be appropriate for the eastern North American (ENA) earthquakes. To examine this effect further, ground motion was simulated for these earthquakes using extended faults with the same bilateral rupture and uniform slip on the fault surface for both constant and increasing stress-drop models. Figure 3 shows the decay of predicted PGA (average of two horizontal components) as a function of closest distance to the seismogenic fault surface. These results illustrate that the ground motion predicted by the increasing stress drop model becomes larger than that predicted using the constant stress-drop model as M_w increases above 6.5. These results incorporate only the response of the direct and primary reflected phases.

In Figure 3, the ground motions appear to have a slower decay with increasing magnitude, resulting in a different fall-off rate for each magnitude. In addition, the ground motions do not decay continuously with increasing distance. A distinct increase in amplitude is predicted for $Mw = 6.5$ magnitude at 50 km and is caused by the critical reflections from internal interfaces. Such an increase in amplitude, although not as dramatic, is predicted at a closer distance (30 km) for the $M_w = 7.5$ earthquake. This variation is related to the fault size because the rays leave the fault surface from different locations. The contributions from these rays vary at different receiving sites since they can either be from a direct or a reflected wave. Figure 4 shows simulated east-west component accelerograms computed for individual ray types at three sites lying in a profile at closest distances of 10, 110 and 159 km respectively from a $M_w = 7.5$ magnitude earthquake. The corresponding sites are S012, S124 and S164 (Figure 4). The accelerograms DIR were simulated using only the direct waves from each sub fault. Likewise, the accelerograms DW1 were computed using all sub fault contributions with only one reflection from the Moho discontinuity. The accelerograms DW2 had two bounces from the Moho discontinuity. For each site, the upper cumulative accelerogram is obtained by summing the contributions DIR and DW1, and the lower accelerogram is obtained by adding contribution DW2 to this sum. Clearly, the direct wave dominates at 10 km. The Moho reflections (DW1) are the most dominant contributions at 110 km. But further away at 159 km, both DW1 and DW2 (two bounces from the Moho discontinuity) are equally strong.

In addition to the crustal structure and source scaling law, the results of the predicted ground motion are expected to depend on the slip distribution across the fault surface. In a recent study, Herrmann and Jost (1988) presented an asperity model used in simulating long-period ground motions from a large New Madrid earthquake ($M_s = 8.4$). Using their asperity model, we have simulated high-frequency ground motions for a $M_w = 7.5$ earthquake (Figure 5). Also shown are the PGA attenuation for $M_w = 7.0$ and $M_w = 6.5$ earthquakes. The slip models were randomly chosen for these

two earthquakes. The results are quite similar to the case of a uniform slip model shown in Figure 3. The magnitude $M_w = 6.5$ earthquake shows a more pronounced effect from crustal reflections, where the effect of both DW1 and DW2 is observed in the attenuation of ground motions. In Figure 6, we show the average attenuation curves for these three earthquakes. The primary characteristic of the attenuation curves is that they tend to flatten with increasing magnitude.

Validation of Simulation Method for Continental-Interior Earthquakes

The New Madrid seismic zone is tectonically classified as a continental-interior region (Nuttli, 1973). For validating the semi-empirical method, we modeled strong motion data from the 1978 Tabas, Iran earthquake (Figure 7, Saikia, 1992), the largest continental-interior earthquake to have produced usable strong motion accelerograms. The slip models KS3 and L1 for both fixed and variable rake angles of Hartzell and Mendoza (1991) and the empirical accelerograms source functions from the Imperial Valley aftershock were used. The time series show good agreement in peak amplitudes, shape and duration of the significant energy, especially for the KS3 slip model with variable rake. Although this study is only one example of this kind, it does provide some confidence for estimating ground motion in a region from a continental-interior earthquake where instrumental strong-motion data are still not available. Another significant result is that close-distance accelerograms of one tectonic regime can be transported to another tectonic regime for use as empirical source functions provided they are corrected for the propagation path of individual recording sites.

Conclusions

Based on the above studies, we make the following conclusions:

(a). The semi-empirical simulation method adopted here was used to simulate the observed accelerograms of the September 1978, Tabas, Iran earthquake, producing a reasonable agreement between data and synthetic accelerograms. Thus, we are confident that the ground motions predicted in this study are reliable estimates for a given slip distribution model.

(b). The peak ground motions from the asperity model are larger than the ground motions predicted by the uniform slip model. In addition, for an individual slip model, the ground motion predicted using the increasing stress-drop source model is larger than the ground motion predicted using the constant stress-drop model, although the discrepancy in the ground motions from the two scaling laws decreases as the magnitude of the event decreases from $M_W = 7.5$ to $M_w = 6.5$.

(c). The effect of lower crustal structure becomes significant at a closest distance of about 40 km from the seismogenic rupture zone. At distances larger than 100 km, the contributions from multiple reflections are also significant.

(d). The effect of attenuation in the embayment sediment is represented in the source function. A careful study of this effect on the ground motion is presently on-going and will be addressed in the final report.

References

Boore, D. M. and G. A. Atkinson (1987). Stochastic prediction of ground motion and spectral response parameters at hard-rock sites in eastern North America, Bull. Seis. Soc. Am., 77, 440-467.

Hartzell, S. and C. Mendoza (1991). Application of iterative least-square waveform inversion of strong motion and teleseismic records to the 1978 Tabas Iran earthquake, Bull. Seis. Soc. Am., 81, 305-331.

Herrmann, R. B. and M.L. Jost (1988). Simulation of long period ground motions for large New Madrid earthquake, in M.A. cassaro and J.D. Cooper, Editors, Seismic Design and Construction of Complex Civil Engineering System, Am. Soc. of Civil Eng., New York, 1-15.

McGarr, A., M. Celebi, E. Sembera, T. Noce, and C. Mueller (1991). Ground motion at the San Francisco international airport from the Loma Prieta earthquake, Bull. Seis. Soc., 81, 1923-1944.

Nuttli, O.W. (1973). Seismic wave attenuation and magnitude relations for eastern North America, J. Geophys. Res., 78, 876-885.

Nuttli, O.W., G.A. Bollinger, and D.W. Griffiths (1979). On the relation between Modified Mercalli Intensity and Body-wave magnitude, Bull. Seis. Soc. Am., 69, 893-909.

Nuttli, O.W. (1983). Average seismic source-parameter relations for mid plate earthquake, Bull. Seis. Soc. Am., 73, 519-535.

Saikia, C.K. (1992). Modeling of strong ground motions from the September 16, 1978 Tabas, Iran earthquake by a semi-empirical method, Bull. Seis. Soc. Am., (manuscript in preparation).

Saikia, C.K., P.G. Somerville, D.V. Helmberger, M. K. Sen, J.P. McLaren, L.J. Burdick, and N.F. Smith (1989). Ground motion attenuation and earthquake source scaling in eastern North America, Electric Power Research Institute, Report.

Somerville, P.G., J.P. McLaren, L.V. LeFevre, R.W. Burger, and D.V. Helmberger (1987). Comparison of source scaling relations of eastern and western North American earthquakes, Bull. Seis. Soc. Am., 77, 322-346.

Somerville, P. G. and J. Yoshimura (1990). The influence of critical moho reflections on strong ground motions recorded in San Francisco and Okland d during the 1989 Loma Prieta earthquake, Geophys. Res. Lett., 17, 1203-1206.

Somerville. P.G., M. K. Sen, and B Cohee (1991). Simulation of strong ground motions recorded during the 1985 Michoacan, Mexico and Valapaiso, Chile earthquake, Bull. Seis. Soc. Am., 81, 1-27.

Toro, G.R. and R. K. McGuire (1987). An investigation into earthquake ground motions characteristics in eastern North America, Bull. Seis, Soc. Am., 77, 468-489.

Figure Captions

Figure 1: Figure showing the distribution of 168 seismic stations used in this study. A total of 8 profiles are laid out. The stations are placed on concentric rings with the largest radius being 160 km.

Figure 2: Ray diagram: DIR represents a direct ray path between the source and receiver, DW1 represents a path for a reflected ray from both the Conrad and the Moho discontinuities; and DW2 represents a ray path which is reflected twice from the Moho discontinuity and once from the free surface.

Figure 3: Attenuation of peak ground acceleration (PGA) for $M_w = 7.5$, $M_w = 7.0$, and $M_w = 6.5$ earthquakes predicted using both constant (open triangle) and increasing (solid circle) stress-drop models. Average of the two horizontal components is plotted.

Figure 4: Effect of propagation: Accelerograms are shown for a $M_w = 7.5$ magnitude earthquake at three sites. These sites lie along the profile of station S164 from the center of the network. For

each station, accelerograms were simulated for direct, DW1 and DW2 ray types separately. All accelerograms are displayed after normalizing to the maximum PGA predicted at that site.

Figure 5: Attenuation of peak ground acceleration (PGA) for $M_w = 7.5$, $M_w = 7.0$, and $M_w = 6.5$ earthquakes predicted using constant stress-drop model and slip distribution models containing asperities. Average of the two horizontal components is plotted.

Figure 6: Attenuation curves smoothly fitting the data shown in Figure 6.

Figure 7: Comparison between recorded and simulated ground motions at one station (Dayhook) recorded from the September 1978, Tabas, Iran earthquake. The scaled Imperial Valley aftershock accelerograms were used for empirical source functions. This event produced usable ground motion at two more stations : Bosrooyeh and Tabas. Similar agreement was obtained at Bosrooyeh. The ground motion recorded at Tabas was larger than predicted.

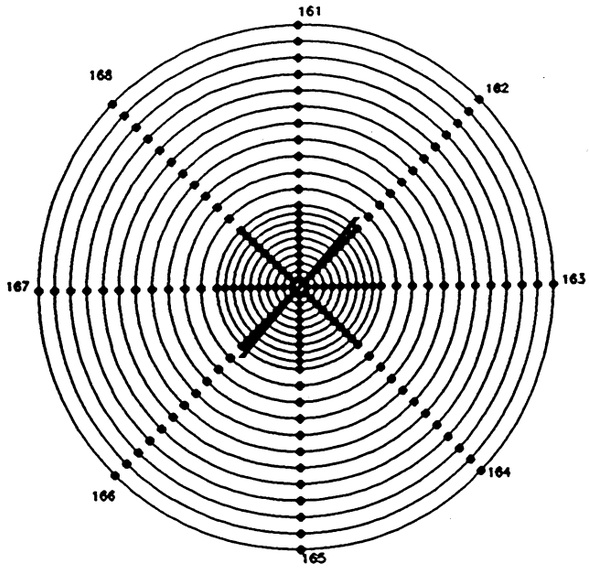

Figure 1

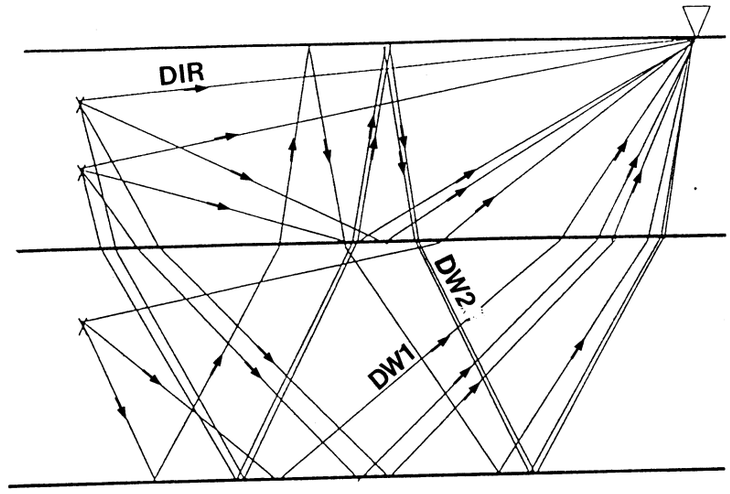

Figure 2

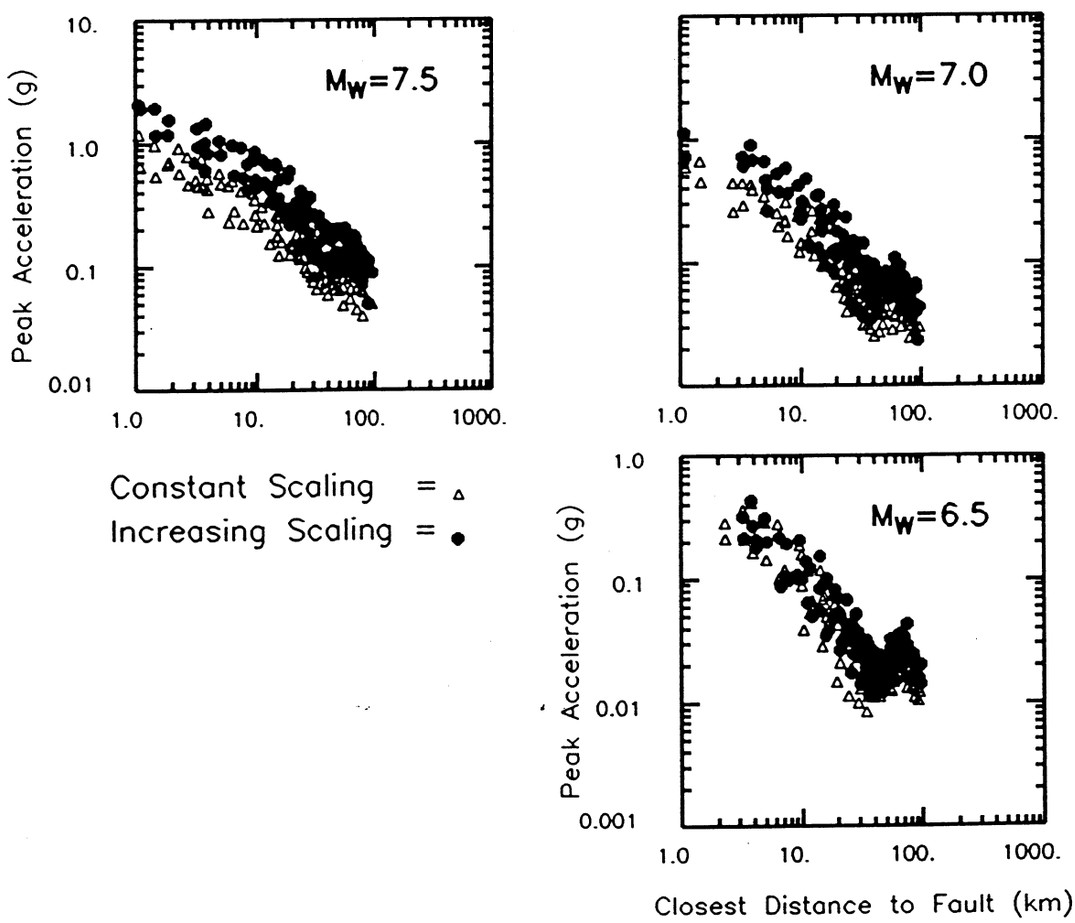

Figure 3

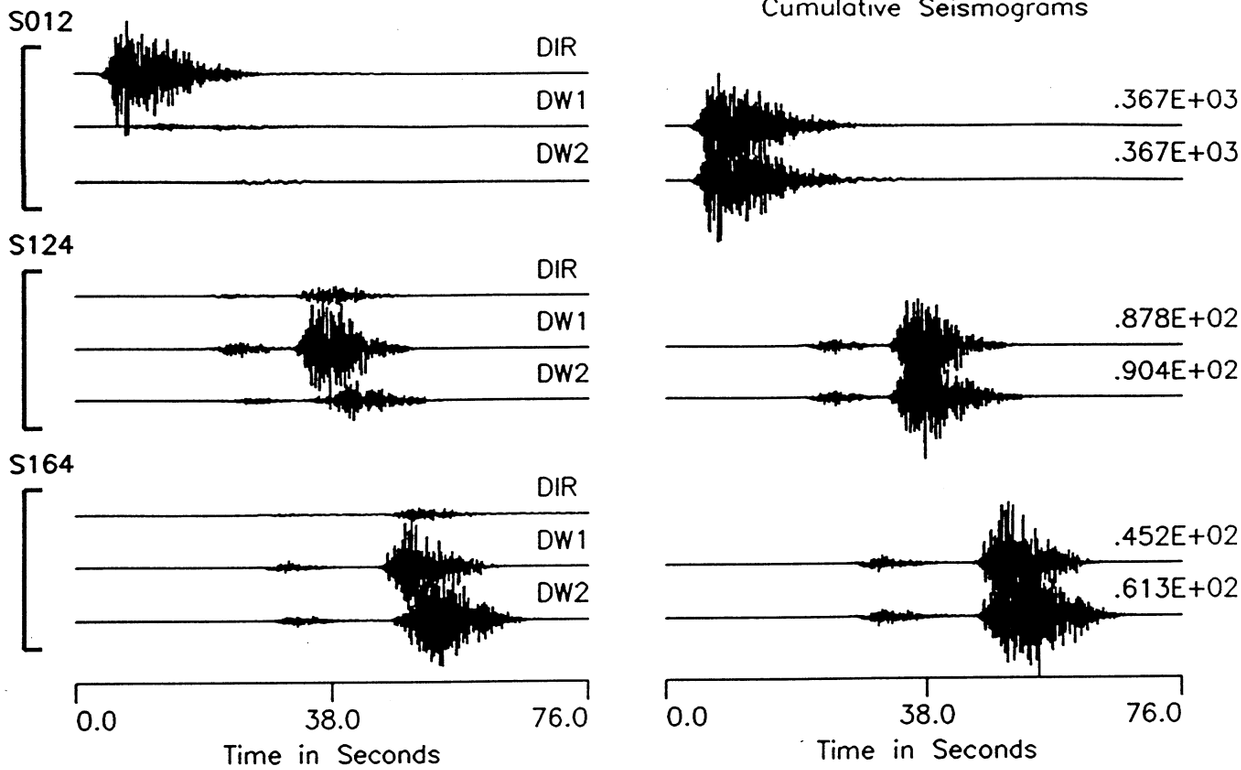

Figure 4

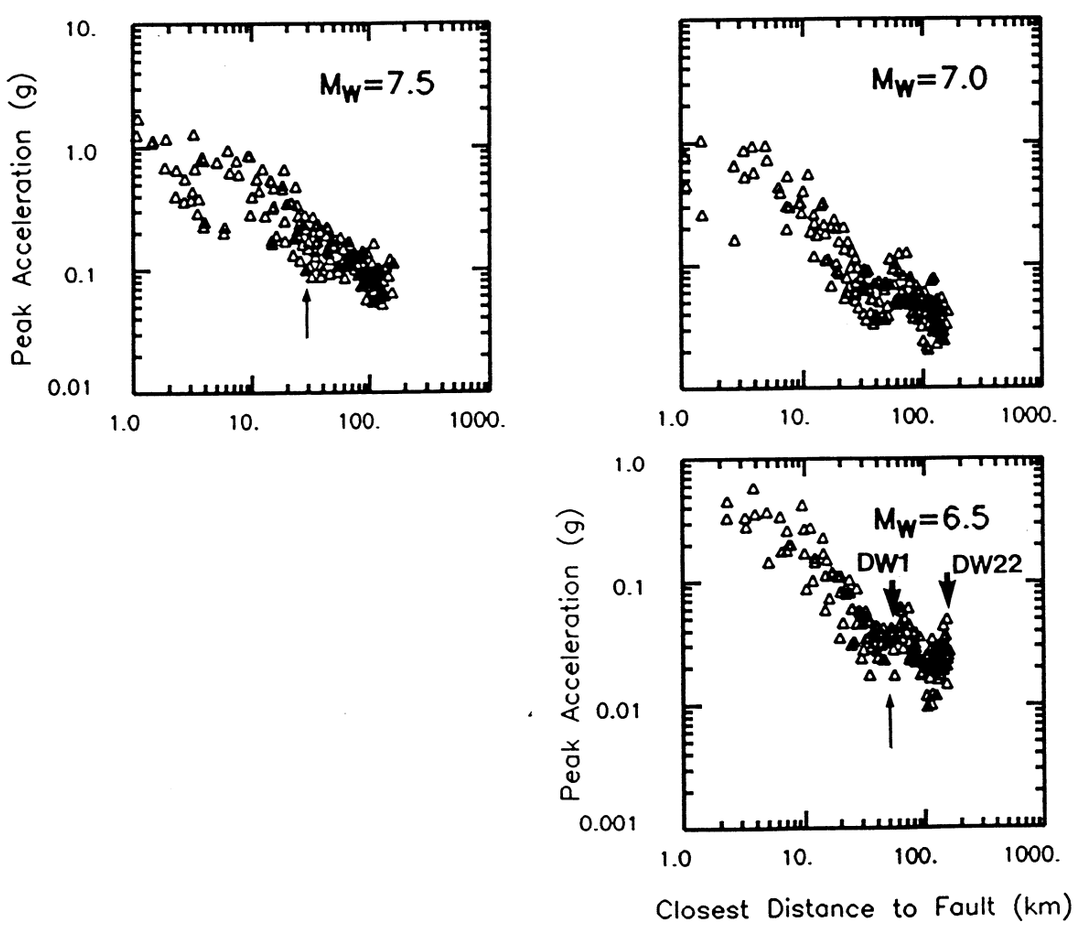

Figure 5

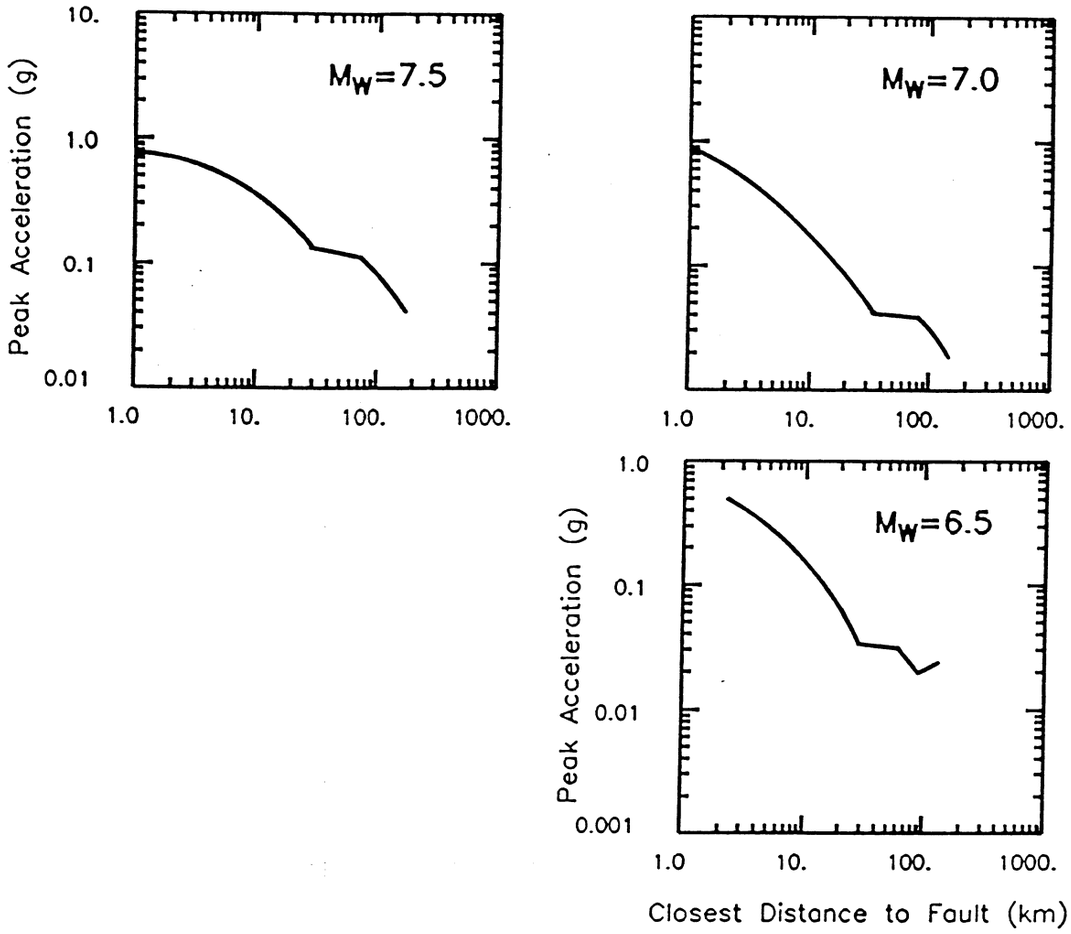

Figure 6

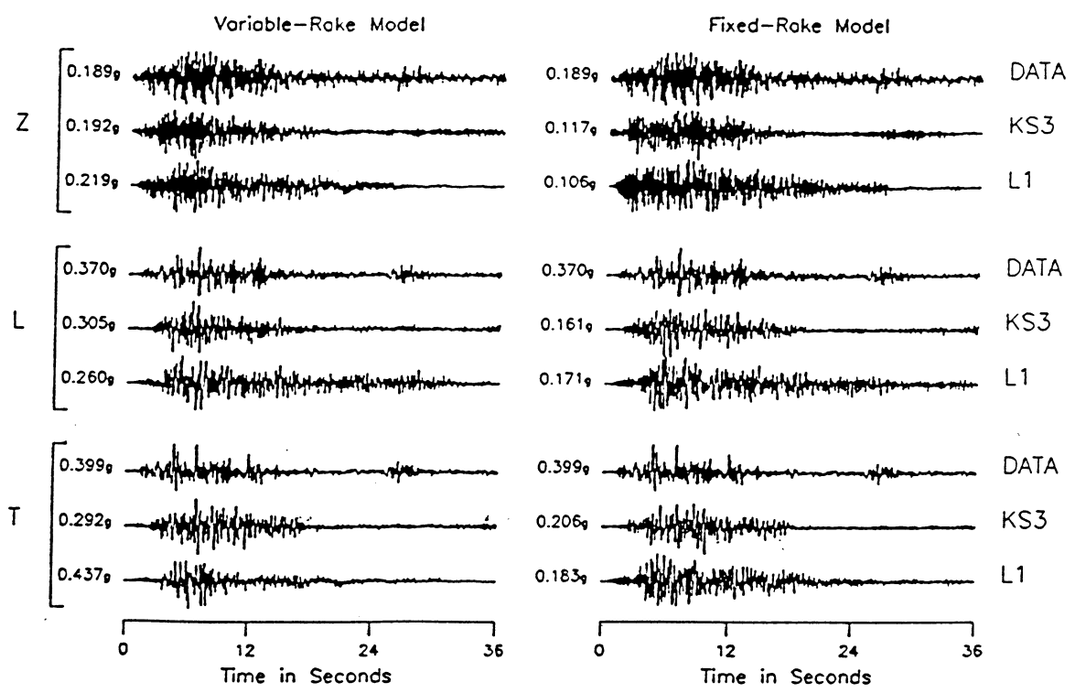

Figure 7